Multisoliton perturbation theory for the Manakov equations and its applications to nonlinear optics

Jianke Yang

Department of Mathematics and Statistics, The University of Vermont, 16 Colchester Avenue, Burlington, Vermont 05401
(Received 2 June 1998)

The effect of small perturbations on the collision of vector solitons in the Manakov equations is studied in this paper. The evolution equations for the soliton parameters (amplitude, velocity, polarization, position, and phases) throughout collision are derived. The method is based on the completeness of the bounded eigenstates of the associated linear operator in L_2 space and a multiple-scale perturbation technique. These results are applied to the coupled nonlinear Schrödinger equations, which govern the pulse propagation in birefringent nonlinear optical fibers. Both transmission and repulsion scenarios are predicted. More interestingly, it is found that, near the transition from transmission to repulsion, the collision outcome is very sensitive to the cross-phase modulational coefficient and initial soliton parameters. Rapid and considerably large oscillations in the parameters of the final vector solitons are observed. All these predictions are confirmed by direct numerical simulations. Applications of these results to ultrafast soliton switching devices are also discussed. [S1063-651X(99)10702-5]

PACS number(s): 42.65.Tg, 41.20.Jb

I. INTRODUCTION

Nonlinear pulse propagation in optical fibers has been studied over 30 years. The idea of using optical solitons as information bits in high-speed telecommunication systems was first proposed in 1973 [1], and then demonstrated experimentally in 1980 [2]. In the following years, as fiber technology advanced, interest in optical soliton transmission started to increase. Multigigabits transmission over more than 10 000 km was reported regularly starting in 1991. To further increase the bit rate and transmission distance, novel techniques such as wavelength division multiplexing (WDM), polarization division multiplexing (PDM), and dispersion management have been proposed and utilized. Various all-optical ultrafast soliton switches have also been designed and demonstrated. These techniques have spurred fresh interest in the theoretical modeling of pulse propagation and collision in the underlying communication systems.

In an ideal fiber, optical solitons can be modeled approximately by the nonlinear Schrödinger (NLS) equation, whose solution behaviors are completely known [3,4]. But in reality, optical fibers are birefringent. Pulses travel at slightly different speeds along the two orthogonal polarization axes. This effect has been analyzed in [5], where two coupled nonlinear Schrödinger (CNLS) equations were derived for the pulse propagation along the two polarization axes. In a linearly birefringent fiber, the cross-phase modulational (XPM) coefficient is 2/3. But it may take other values if the birefringence is elliptic [6]. If the birefringence randomly varies along the fiber due to bending, twisting, and the environmental perturbations, the pulses evolve according to the Manakov equations with corrections caused by polarization mode dispersion [8,9]. The CNLS equations also arise for beam propagation in crystals [10–12]. In this case, the XPM coefficient can be very close to one. Water waves is another field where these equations are relevant [13,14].

Birefringent fibers also support optical solitons (they are

called vector solitons) [7,25]. The collision of vector solitons is critical in many optical switching devices and nonlinear optical telecommunication networks. In all-optical soliton switching, various ultrafast digital logic gates have been proposed and experimentally demonstrated [15,16]. These logic gates utilize the phase or frequency shift created by the collision between orthogonally polarized solitons. They can operate at bit rates up to 0.2 THz. In long haul telecommunication systems, PDM and WDM technology have been explored. In a PDM system, solitons are launched alternately along the fast and slow axes of a birefringent fiber in order to reduce the tail interference of adjacent solitons [17]. This technique could double the transmission rate of a single-wavelength channel with little increase in bit error rate. In a WDM system, multiple channels with finite frequency separations are utilized. This technique could increase the total transmission rate of a communication line by many fold. But when these two techniques are combined, collision between solitons in different channels will arise. This will alter the polarization states of the originally orthogonal solitons, and thus ruin the benefits of the PDM system. In fact, it has been shown recently by experiments and theoretical analysis that the WDM and PDM systems are incompatible [18,19]. In crystals, collision of beams (spatial vector solitons) is also an interesting question. A spatial soliton logic gate based on the interaction of two orthogonally polarized beams has also been proposed [12,20].

Collision of vector solitons in the CNLS equations has been studied before [21,23–25]. If the XPM coefficient is one, the equations are the integrable Manakov equations. The soliton collision is elastic, and the outcome has been explicitly specified [21,22]. But in many situations, this coefficient is not equal to one. Furthermore, small perturbations such as polarization mode dispersion, third-order dispersion, and Raman scattering may also need to be considered. In such cases, the collision is inelastic and more difficult to analyze. In the work [23–25], such small perturbations were neglected, while the XPM coefficient was taken different

from one. In [23], the authors studied this inelastic collision between two orthogonally polarized solitons. They numerically demonstrated the transmission, reflection and fusion scenarios depending on the precollision soliton parameters. They also qualitatively explained some of these scenarios using a simple analytical estimate based on spatial resonance between the two solitons. In [24], this collision was investigated numerically. It was shown that large collision speed causes little radiation, but appreciable changes in the pulse ellipticity. Smaller relative speed gives imperfect collision for nearly orthogonal, linearly polarized pulses. In [25], we showed that the CNLS equations support many types of vector solitons. Only the single-hump ones are stable. Using a NLS soliton in a slowly varying potential model, we explained certain types of transmission and reflection behaviors. We also showed numerically that collision of two vector solitons could create one or more new vector solitons if the XPM coefficient is large.

Despite the above efforts, a rigorous analytical theory describing the collision process has still been lacking. In this paper, we present such an analytical theory. We study the collision of two vector solitons, based on the perturbed Manakov equations:

$$iA_t + A_{xx} + (|A|^2 + |B|^2)A = \epsilon M(A, B, \partial_x, \partial_t), \quad (1.1a)$$

$$iB_t + B_{xx} + (|B|^2 + |A|^2)B = \epsilon N(A, B, \partial_x, \partial_t). \quad (1.1b)$$

Here A and B are complex functions, and $\epsilon \ll 1$. When $\epsilon = 0$, Eqs. (1.1) are the integrable Manakov equations. Vector solitons collide with each other elastically, except that their polarizations may change after collision. If the incoming vector solitons have the same or orthogonal polarizations, such change will not occur. When $\epsilon \ll 1$, Eqs. (1.1) are the perturbed Manakov equations. Generally, all the soliton parameters will change after collision. Three types of analytical approaches are known for studying the dynamics of solitons and their collisions in perturbed integrable systems. They are the variational principle method, the direct perturbation technique based on a Green's function, and the perturbed inverse scattering method. These methods have been comprehensively reviewed in [26]. Some of the recent contributions can be found in [27–30]. As far as soliton collision is concerned, these methods have been applied to the KdV, modified KdV, NLS, sine-Gordon, and Benjamin-Ono equations under perturbations [26,28]. Collision scenarios, such as fusion of a soliton pair into a breather and transmissive collision, have been analyzed in detail. The perturbation theory for a single soliton of the Manakov system has also been developed [9,31,32].

In the present paper, we study the soliton collision in the perturbed Manakov equations. Our method is based on the closure of the bounded eigenstates of the associated linear operator and a direct perturbation technique (see [33,29,30]). We first construct the exact two-soliton solution of the Manakov equations by the Hirota method. Then, we employ this perturbation technique to the colliding vector solitons under perturbations, and derive the evolution equations for the amplitudes, velocities, polarizations, positions, and phases of the two colliding solitons. Integration of these evolution equations will give these soliton parameters through-

out the collision. Such information is valuable for understanding the collision process of vector solitons in the presence of perturbations. As an example, we consider the CNLS equation with the XPM coefficient close to 1, and study in detail the collision of two orthogonally polarized solitons. We find that both transmission and reflection scenarios can occur. Transmission typically happens when the XPM coefficient or the collision speed is larger than certain critical values. Reflection arises when the opposite conditions are true. In both cases, the soliton parameters are changed considerably after collision. More interestingly, when the collision changes from transmission to repulsion, the parameters of the outcoming solitons are very sensitive to those of the incoming solitons and the XPM coefficient. Rapid and appreciable oscillations in the parameters of the outcoming solitons are observed just before and after the transition. All these theoretical predictions are confirmed by our direct numerical simulations. We also find, through numerical calculations, that two colliding solitons can also fuse into one, or new vector solitons can be created, after collision. This may happen when the XPM coefficient is not close to one, which lies outside the regime of the current perturbation theory. In the end, we discuss the implications of these results to digital soliton logic gates, and propose a soliton-repulsion logic gate using birefringent fibers.

This paper is organized as follows. In Sec. II, we determine the exact two-soliton solution of the Manakov equations by the Hirota method. In Sec. III, we derive the evolution equations for the soliton parameters throughout collision for the perturbed Manakov equations. In Sec. IV, we apply these results to the CNLS equation. In particular, we study the collision of two orthogonally polarized solitons, and discuss the analytical and numerical results in detail. In Sec. V, we summarize the main results obtained in the previous sections, and explore their applications to soliton switching devices.

II. EXACT TWO-SOLITON SOLUTIONS IN THE MANAKOV EQUATIONS

When ϵ is zero, Eqs. (1.1) are the Manakov equations, which allow exact N-soliton solutions. These solutions can be determined by Hirota's method. The two-soliton solution has been given by Radhakrishnan *et al.* [22]. For the convenience of the present analysis, we will explicitly introduce the polarization and phase variables of the solitons, and reformulate their solution.

The one-soliton solution of the Manakov equations is given by

$$\begin{bmatrix} A \\ B \end{bmatrix} = \begin{bmatrix} \cos\theta e^{i\delta} \\ \sin\theta e^{-i\delta} \end{bmatrix} \frac{e^\eta}{1 + e^{\eta + \eta^*}}, \quad (2.1)$$

where

$$\eta = ax + ia^2 t + \eta_0, \quad (2.2)$$

$$a = r + iv, \quad \eta_0 = \xi_0 + i\zeta_0, \quad (2.3)$$

and r, v, θ, δ, ξ_0, and ζ_0 are real constants. This soliton can be rewritten as

$$\begin{bmatrix} A \\ B \end{bmatrix} = \begin{bmatrix} \cos\theta e^{i\delta} \\ \sin\theta e^{-i\delta} \end{bmatrix} \sqrt{2}re^{i\{vx+(r^2-v^2)t+\zeta_0\}} \operatorname{sech}\{r(x-2vt)$$
$$+ \xi_0\}. \tag{2.4}$$

We can see that it has amplitude $\sqrt{2}r$, velocity $2v$, polarization θ, initial central position $-\xi_0/r$, in-phase constant ζ_0, and opposite phase constant δ.

The two-soliton solution is given by

$$A = \frac{\alpha_1 e^{\eta_1} + \alpha_2 e^{\eta_2} + e^{\eta_1+\eta_1^*+\eta_2+S_1} + e^{\eta_1+\eta_2+\eta_2^*+S_2}}{1 + e^{\eta_1+\eta_1^*+R_1} + e^{\eta_1+\eta_2^*+S_0} + e^{\eta_1^*+\eta_2+S_0^*} + e^{\eta_2+\eta_2^*+R_2} + e^{\eta_1+\eta_1^*+\eta_2+\eta_2^*+R_3}}, \tag{2.5a}$$

$$B = \frac{\beta_1 e^{\eta_1} + \beta_2 e^{\eta_2} + e^{\eta_1+\eta_1^*+\eta_2+S_1'} + e^{\eta_1+\eta_2+\eta_2^*+S_2'}}{1 + e^{\eta_1+\eta_1^*+R_1} + e^{\eta_1+\eta_2^*+S_0} + e^{\eta_1^*+\eta_2+S_0^*} + e^{\eta_2+\eta_2^*+R_2} + e^{\eta_1+\eta_1^*+\eta_2+\eta_2^*+R_3}}, \tag{2.5b}$$

where

$$\eta_k = a_k x + i a_k^2 t + \eta_{k0}, \tag{2.6}$$

$$a_k = r_k + i v_k, \quad \eta_{k0} = \xi_{k0} + i\zeta_{k0}, \tag{2.7}$$

$$\alpha_k = \cos\theta_k e^{i\delta_k}, \quad \beta_k = \sin\theta_k e^{-i\delta_k}, \tag{2.8}$$

$$e^{R_1} = \frac{\kappa_{11}}{a_1+a_1^*}, \quad e^{R_2} = \frac{\kappa_{22}}{a_2+a_2^*}, \quad e^{S_0} = \frac{\kappa_{12}}{a_1+a_2^*}, \tag{2.9}$$

$$e^{R_3} = \frac{|a_1-a_2|^2}{(a_1+a_1^*)(a_2+a_2^*)|a_1+a_2^*|^2}(\kappa_{11}\kappa_{22}-\kappa_{12}\kappa_{21}), \tag{2.10}$$

$$\begin{bmatrix} e^{S_1} \\ e^{S_1'} \end{bmatrix} = \frac{a_1-a_2}{(a_1+a_1^*)(a_1^*+a_2)}\left(\begin{bmatrix} \alpha_1 \\ \beta_1 \end{bmatrix}\kappa_{21} - \begin{bmatrix} \alpha_2 \\ \beta_2 \end{bmatrix}\kappa_{11}\right), \tag{2.11}$$

$$\begin{bmatrix} e^{S_2} \\ e^{S_2'} \end{bmatrix} = \frac{a_2-a_1}{(a_2+a_2^*)(a_1+a_2^*)}\left(\begin{bmatrix} \alpha_2 \\ \beta_2 \end{bmatrix}\kappa_{12} - \begin{bmatrix} \alpha_1 \\ \beta_1 \end{bmatrix}\kappa_{22}\right), \tag{2.12}$$

and

$$\kappa_{ij} = \frac{\alpha_i\alpha_j^* + \beta_i\beta_j^*}{2(a_i+a_j^*)}. \tag{2.13}$$

If we assume that the two solitons have different velocities, say, $v_1 > v_2$, then as $t \to -\infty$, this solution reduces to two separate one-solitons:

$$\begin{bmatrix} A_h \\ B_h \end{bmatrix} \to \begin{bmatrix} \cos\theta_1 e^{i\delta_1} \\ \sin\theta_1 e^{-i\delta_1} \end{bmatrix}\frac{e^{\bar{\eta}_1}}{1+e^{\bar{\eta}_1+\bar{\eta}_1^*}} + \begin{bmatrix} \cos\bar{\theta}_2 e^{i\bar{\delta}_2} \\ \sin\bar{\theta}_2 e^{-i\bar{\delta}_2} \end{bmatrix}\frac{e^{\bar{\eta}_2}}{1+e^{\bar{\eta}_2+\bar{\eta}_2^*}}, \tag{2.14}$$

where

$$\bar{\eta}_k = a_k x + i a_k^2 t + \bar{\eta}_{k0}, \quad \bar{\eta}_{k0} = \bar{\xi}_{k0} + i\bar{\zeta}_{k0}, \tag{2.15}$$

$$s_1 e^{i\gamma_1} = e^{S_1}/\sqrt{|e^{S_1}|^2 + |e^{S_1'}|^2}, \quad s_1' e^{i\gamma_1'} = e^{S_1'}/\sqrt{|e^{S_1}|^2 + |e^{S_1'}|^2}, \tag{2.16}$$

$$\bar{\eta}_{10} = \eta_{10} - \ln 2\sqrt{2}r_1, \tag{2.17}$$

$$\bar{\eta}_{20} = \eta_{20} + \tfrac{1}{2}\ln(|e^{S_1}|^2 + |e^{S_1'}|^2) - \ln 2\sqrt{2}r_2 + \tfrac{1}{2}i(\gamma_1+\gamma_1'), \tag{2.18}$$

$$\cos\bar{\theta}_2 = s_1, \quad \sin\bar{\theta}_2 = s_1', \tag{2.19}$$

$$\bar{\delta}_2 = \delta_2 + \tfrac{1}{2}(\gamma_1 - \gamma_1'). \tag{2.20}$$

We would like to remind the reader that, in the above two-soliton solutions, $\{a_k, \eta_{k0}, \theta_k, \delta_{ki}, k=1,2\}$ are the intermediate parameters. The two separate solitons (2.14) actually have amplitudes $\sqrt{2}r_k$, velocities $2v_k$, polarizations $\theta_1(\bar{\theta}_2)$, initial positions $-\bar{\xi}_{k0}/r_k$, in-phase constants $\bar{\zeta}_{k0}$, and opposite phase constants $\delta_1(\bar{\delta}_2)$, respectively. It is easy to show that, if these actual parameters of the initial solitons are given, then the intermediate parameters θ_2 and δ_2 are determined from the equation,

$$\cot\theta_2 e^{2i(\delta_2-\delta_1)}$$
$$= -\frac{\tfrac{1}{2}\sin 2\theta_1\tan\bar{\theta}_2 - (\sin^2\theta_1 - D)e^{2i(\bar{\delta}_2-\delta_1)}}{\tan\bar{\theta}_2(\cos^2\theta_1 - D) - \tfrac{1}{2}\sin 2\theta_1 e^{2i(\bar{\delta}_2-\delta_1)}}, \tag{2.21}$$

where

$$D = \frac{a_1^*+a_2}{a_1+a_1^*},$$

and the values of η_{k0} are obtained from Eqs. (2.17) and (2.18), respectively.

As $t \to \infty$, the two-soliton solution (2.5) also reduces to two separate one-solitons:

$$\begin{bmatrix} A_h \\ B_h \end{bmatrix} \to \begin{bmatrix} \cos\hat{\theta}_1 e^{i\hat{\delta}_1} \\ \sin\hat{\theta}_1 e^{-i\hat{\delta}_1} \end{bmatrix}\frac{e^{\hat{\eta}_1}}{1+e^{\hat{\eta}_1+\hat{\eta}_1^*}} + \begin{bmatrix} \cos\theta_2 e^{i\delta_2} \\ \sin\theta_2 e^{-i\delta_2} \end{bmatrix}\frac{e^{\hat{\eta}_2}}{1+e^{\hat{\eta}_2+\hat{\eta}_2^*}}, \tag{2.22}$$

where the quantities with carets are given by relations similar to Eqs. (2.15)–(2.20), with the bars replaced by carets, and the indices 1 and 2 in them switched. Notice that after colli-

sion, the solitons pass through each other. Their amplitudes and velocities do not change, but the polarizations, phases, and positions are shifted. These shifted values can be obtained directly from the precollision soliton parameters. For this purpose, we define the unit vector

$$\mathbf{c} = \begin{bmatrix} \cos\theta e^{i(\zeta_0+\delta)} \\ \sin\theta e^{i(\zeta_0-\delta)} \end{bmatrix} \qquad (2.23)$$

for a soliton (2.1). This vector determines the soliton's polarization and phases. From the asymptotic relations (2.14) and (2.22) of the two-soliton solution (2.5), it is easy to verify that

$$\mathbf{c}_1^+ = \frac{1}{\chi} \frac{a_1^*+a_2}{a_1^*-a_2^*} \left[\mathbf{c}_1^- + \frac{a_2+a_2^*}{a_1^*-a_2^*} (\mathbf{c}_2^{-*}\cdot\mathbf{c}_1^-)\mathbf{c}_2^- \right], \qquad (2.24a)$$

$$\mathbf{c}_2^+ = \frac{1}{\chi} \frac{a_1^*+a_2}{a_2-a_1} \left[\mathbf{c}_2^- + \frac{a_1+a_1^*}{a_2-a_1} (\mathbf{c}_1^{-*}\cdot\mathbf{c}_2^-)\mathbf{c}_1^- \right], \qquad (2.24b)$$

where

$$\chi = \left| \frac{a_1+a_2^*}{a_1-a_2} \right| \left[1 + \frac{(a_1+a_1^*)(a_2+a_2^*)}{|a_1-a_2|^2} |\mathbf{c}_1^{-*}\cdot\mathbf{c}_2^-|^2 \right]^{1/2}, \qquad (2.25)$$

and $\mathbf{c}_k^-$ and $\mathbf{c}_k^+$ ($k=1,2$) are the just defined unit vectors for the precollision and after-collision solitons, respectively (see also [21]). These relations will readily give the shifted polarization and phase values. It is clear from Eqs. (2.24) that the soliton polarizations do not change; only in the case when their initial polarizations are parallel ($\mathbf{c}_1^- \| \mathbf{c}_2^-$, i.e., $\theta_1^- = \theta_2^-$, and $|\delta_1^- - \delta_2^-| = 0$ or π), or orthogonal ($\mathbf{c}_1^- \perp \mathbf{c}_2^-$, i.e., $|\theta_1^- - \theta_2^-| = \pi/2$). The position shifts of the colliding solitons are also easy to obtain. Suppose that $v_1 > v_2$. Then these shifts can be derived from Eqs. (2.14) and (2.22) as

$$\Delta x_1 = \frac{\ln\chi}{r_1}, \quad \Delta x_2 = -\frac{\ln\chi}{r_2}. \qquad (2.26)$$

In the rest of this paper, we will treat the two-soliton solutions A_h and B_h as functions of the initial soliton parameters [see Eqs. (2.14)],

$$\begin{bmatrix} A_h \\ B_h \end{bmatrix} = \begin{bmatrix} A_h \\ B_h \end{bmatrix} (r_1, v_1, \bar{\xi}_1, \bar{\zeta}_1, \theta_1, \delta_1, r_2, v_2, \bar{\xi}_2, \bar{\zeta}_2, \bar{\theta}_2, \bar{\delta}_2), \qquad (2.27)$$

where $\bar{\xi}_k$ and $\bar{\zeta}_k$ ($k=1,2$) are real functions,

$$\bar{\xi}_k + i\bar{\zeta}_k = ia_k^2 t + \bar{\eta}_{k0}, \qquad (2.28)$$

i.e.,

$$\bar{\xi}_k = -2r_k v_k t + \bar{\xi}_{k0}, \quad \bar{\zeta}_k = (r_k^2 - v_k^2)t + \bar{\zeta}_{k0}. \qquad (2.29)$$

Thus, before collision, the solitons have amplitudes $\sqrt{2}r_k$, velocities $2v_k$, polarizations $\theta_1(\bar{\theta}_2)$, central locations $-\bar{\xi}_k/r_k$, in phases $\bar{\zeta}_k$, and opposite phases $\delta_1(\bar{\delta}_2)$, respectively. Furthermore, for convenience, we will drop the bars.

III. COLLIDING VECTOR SOLITONS UNDER PERTURBATIONS

When $\epsilon \ll 1$, the colliding soliton solution can be expanded into a perturbation series,

$$A = A_h(r_k, v_k, \xi_k, \zeta_k, \theta_k, \delta_k, \ k=1,2) + \epsilon A_1 + \epsilon^2 A_2 + \cdots, \qquad (3.1a)$$

$$B = B_h(r_k, v_k, \xi_k, \zeta_k, \theta_k, \delta_k, \ k=1,2) + \epsilon B_1 + \epsilon^2 B_2 + \cdots, \qquad (3.1b)$$

where

$$\xi_k = -2\int_0^t r_k v_k dt + \xi_{k0}, \qquad (3.2a)$$

$$\zeta_k = \int_0^t (r_k^2 - v_k^2)dt + \zeta_{k0}. \qquad (3.2b)$$

Due to the small perturbations, the soliton parameters r_k, v_k, ξ_{k0}, ζ_{k0}, θ_k, and δ_k will be forced to vary. In the following, we derive the evolution equations for the soliton parameters throughout collision. The method we will use is based on the completeness of the bounded eigenstates of the associated linear operator and a multiple-scale perturbation procedure.

When Eqs. (3.1) are substituted into Eqs. (1.1), the zeroth-order equations are trivially satisfied since A_h and B_h are the exact two-soliton solutions of the Manakov equations. At order ϵ, we get

$$L\Phi = R - W, \qquad (3.3)$$

where

$$L = i\partial_t + \begin{pmatrix} \sigma_3 & \\ & \sigma_3 \end{pmatrix} H, \qquad (3.4)$$

$$H = \begin{pmatrix} 2|A_h|^2+|B_h|^2 & A_h^2 & A_h B_h^* & A_h B_h \\ A_h^{*2} & 2|A_h|^2+|B_h|^2 & A_h^* B_h^* & A_h^* B_h \\ A_h^* B_h & A_h B_h & 2|B_h|^2+|A_h|^2 & B_h^2 \\ A_h^* B_h^* & A_h B_h^* & B_h^{*2} & 2|B_h|^2+|A_h|^2 \end{pmatrix}, \qquad (3.5)$$

which is a Hermitian matrix,

$$\Phi = (A_1, A_1^*, B_1, B_1^*)^T, \qquad (3.6)$$

$$R = (M, -M^*, N, -N^*)^T, \qquad (3.7)$$

$$W = i \sum_{k=1}^{2} \{ \Psi_{r_k} r_{kT} + \Psi_{v_k} v_{kT} + \Psi_{\xi_k} \xi_{k0T} + \Psi_{\zeta_k} \zeta_{k0T} + \Psi_{\theta_k} \theta_{kT}$$

$$+ \Psi_{\delta_k} \delta_{kT} \}, \qquad (3.8)$$

$$\Psi = (A_h, A_h^*, B_h, B_h^*)^T. \qquad (3.9)$$

Here, $\sigma_3 = \mathrm{diag}(1, -1)$ is the third Pauli spin matrix, the subscript T is the derivative with respect to the slow time ϵt, and the superscript T represents the transpose of a matrix.

Even though the linear operator L in Eq. (3.3) is a partial differential operator with variable coefficients, Eq. (3.3) can still be solved. Here the key idea is to establish the completeness of the bounded eigenstates of L in L_2 space, and define an appropriate inner product. We first study the null space of L. Recall that the two-soliton solution (2.5) has 12 free parameters. The derivatives of Ψ with respect to each of these parameters, i.e.,

$$\{ \tilde{\Psi}_{r_k}, \tilde{\Psi}_{v_k}, \Psi_{\xi_k}, \Psi_{\zeta_k}, \Psi_{\theta_k}, \Psi_{\delta_k}, \quad k=1,2 \} \qquad (3.10)$$

span the discrete subspace of this null space. Here,

$$\tilde{\Psi}_{r_k} = \Psi_{r_k} - 2t(v_k \Psi_{\xi_k} - r_k \Psi_{\zeta_k}), \qquad (3.11)$$

$$\tilde{\Psi}_{v_k} = \Psi_{v_k} - 2t(r_k \Psi_{\xi_k} + v_k \Psi_{\zeta_k}). \qquad (3.12)$$

The continuous subspace consists of eigenfunctions $\Phi_c(x,t,\lambda)$, which are oscillatory at infinity. Here the parameter λ is the wave number of the function at infinity, which characterizes the continuous eigenfunction.

The above discrete and continuous eigenfunctions form a complete set. This has been shown in [33]. We define the inner product as

$$(\psi_1, \psi_2) = \int_{-\infty}^{\infty} \psi_1^{*T} \begin{pmatrix} \sigma_3 & \\ & \sigma_3 \end{pmatrix} \psi_2 \, dx. \qquad (3.13)$$

Then, if ψ_1 and ψ_2 are in L's null space, i.e.,

$$\psi_{kt} = i \begin{pmatrix} \sigma_3 & \\ & \sigma_3 \end{pmatrix} H \psi_k, \quad k=1,2; \qquad (3.14)$$

then, it is easy to show that

$$\frac{d}{dt}(\psi_1, \psi_2) = 0. \qquad (3.15)$$

In the proof of this relation, the fact that H is Hermitian has been used.

We see from Eq. (3.15) that, to evaluate the inner products of two functions in L's null space, we can take $t \rightarrow -\infty$. Recall that, in this limit, the two-soliton solution (2.5) reduces to two separate one-solitons [see Eqs. (2.14)]. Thus, L's eigenfunctions are also simplified to those of the linear-

ization operator around a single soliton, which have been discussed before [9]. In this way, we can show that the discrete and continuous eigenfunctions in the null space of L are orthogonal to each other. Furthermore, the nonzero inner products of the discrete eigenfunctions are

$$(\tilde{\Psi}_{r_k}, \Psi_{\zeta_k}) = (\Psi_{\zeta_k}, \tilde{\Psi}_{r_k})^* = 4i, \qquad (3.16a)$$

$$(\tilde{\Psi}_{v_k}, \Psi_{\xi_k}) = (\Psi_{\xi_k}, \tilde{\Psi}_{v_k})^* = 4i, \qquad (3.16b)$$

$$(\tilde{\Psi}_{r_k}, \Psi_{\delta_k}) = (\Psi_{\delta_k}, \tilde{\Psi}_{r_k})^* = 4i \cos 2\theta_k, \qquad (3.16c)$$

$$(\Psi_{\theta_k}, \Psi_{\delta_k}) = (\Psi_{\delta_k}, \Psi_{\theta_k})^* = -8i r_k \sin 2\theta_k. \qquad (3.16d)$$

Here, $k=1$ and 2. Notice that the basis $\tilde{\Psi}_{r_k}$ and $\tilde{\Psi}_{v_k}$ have a secular term proportional to t. To avoid such an undesirable behavior, we use instead the equivalent set

$$\{ \Psi_{r_k}, \Psi_{v_k}, \Psi_{\xi_k}, \Psi_{\zeta_k}, \Psi_{\theta_k}, \Psi_{\delta_k}, \quad k=1,2 \}, \qquad (3.17)$$

which also spans the discrete subspace. The nonzero inner products between them take the same form as Eqs. (3.16), with $\tilde{\Psi}_{r_k}$ and $\tilde{\Psi}_{v_k}$ replaced by $\tilde{\Psi}_{r_k}$ and Ψ_{v_k}, respectively.

Now, we are ready to solve the linear equation (3.3) by expanding the solution Φ and the forcing term $R - W$ into this complete set of L's eigen-functions:

$$\Phi = \sum_{k=1}^{2} \{ c_{1k} \Psi_{r_k} + c_{2k} \Psi_{v_k} + c_{3k} \Psi_{\xi_k} + c_{4k} \Psi_{\zeta_k}$$

$$+ c_{5k} \Psi_{\theta_k} + c_{6k} \Psi_{\delta_k} \} + \int C_\lambda \Phi_c(x,t,\lambda) d\lambda, \qquad (3.18)$$

$$R - W = \sum_{k=1}^{2} \{ d_{1k} \Psi_{r_k} + d_{2k} \Psi_{v_k} + d_{3k} \Psi_{\xi_k} + d_{4k} \Psi_{\zeta_k}$$

$$+ d_{5k} \Psi_{\theta_k} + d_{6k} \Psi_{\delta_k} \} + \int D_\lambda \Phi_c(x,t,\lambda) d\lambda. \qquad (3.19)$$

Here, the c_{nk}'s and C_λ are functions of t. Using the inner products of the equivalent set (3.17) to Eq. (3.19), we can determine the expansion coefficients d_{nk} from the following equations:

$$r_{kT} + i d_{1k}^* = \tfrac{1}{4}(R, \Psi_{\zeta_k}), \qquad (3.20a)$$

$$v_{kT} + i d_{2k}^* = \tfrac{1}{4}(R, \Psi_{\xi_k}), \qquad (3.20b)$$

$$\xi_{k0T} + i d_{3k}^* = -\tfrac{1}{4}(R, \Psi_{v_k}), \qquad (3.20c)$$

$$\zeta_{k0T} + i d_{4k}^* + \cos 2\theta_k (\delta_{kT} + i d_{6k}^*) = -\tfrac{1}{4}(R, \Psi_{r_k}), \qquad (3.20d)$$

$$\cos 2\theta_k (r_{kT} + i d_{1k}^*) - 2r_k \sin 2\theta_k (\theta_{kT} + i d_{5k}^*) = \tfrac{1}{4}(R, \Psi_{\delta_k}), \qquad (3.20e)$$
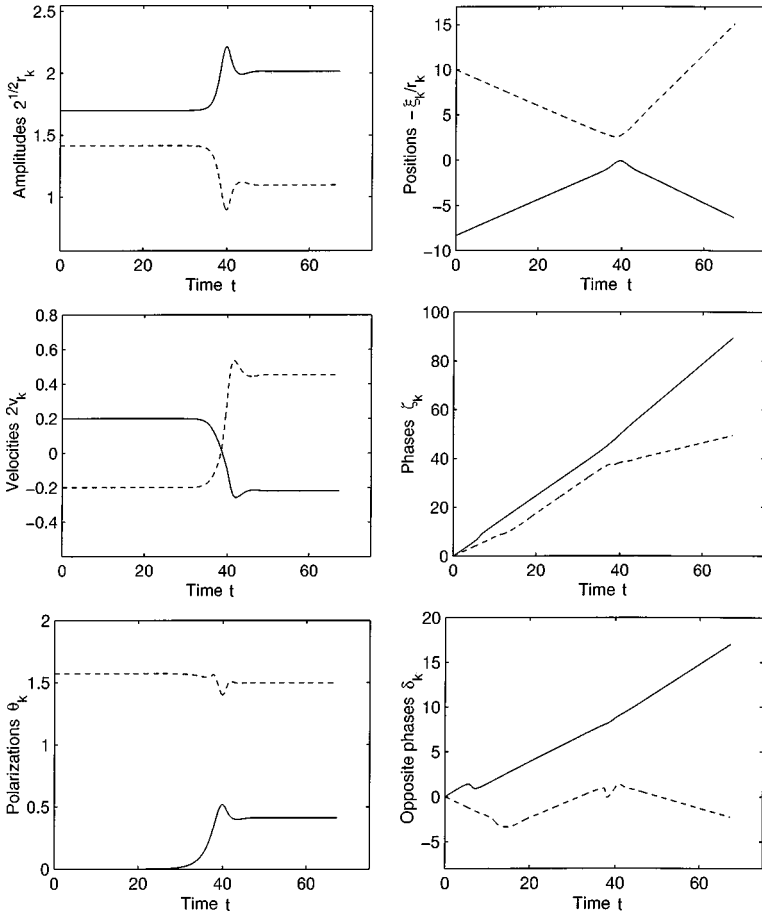
FIG. 1. Time evolution of soliton parameters throughout collision for $\beta = 2/3$ and $v = 0.4$, predicted analytically by Eqs. (4.3). The solid and dashed curves are for the two different vector solitons.

$$\delta_{kT} + id^*_{6k} = \frac{(R, \Psi_{\theta_k})}{8 r_k \sin 2\theta_k}. \tag{3.20f}$$

When we substitute the two expansions (3.18) and (3.19) into Eq. (3.3) and compare the coefficients of the discrete eigenfunctions, we find that the evolution equations for the coefficients c_{nk} in Eq. (3.18) are

$$ic'_{nk} = d_{nk}, \quad n = 1,2,5,6, \tag{3.21a}$$

$$i(c'_{3k} + 2v_k c_{1k} + 2r_k c_{2k}) = d_{3k}, \tag{3.21b}$$

$$i(c'_{4k} - 2r_k c_{1k} + 2v_k c_{2k}) = d_{4k}, \tag{3.21c}$$

where $k = 1$ and 2, and the prime represents the derivative with respect to t. Notice that, as $t \to \infty$, the forcing terms d_{nk} can be easily calculated from Eqs. (3.20) using the asymptotic forms of A_h and B_h given in Eq. (2.22). If the perturbation R does not depend on t explicitly, then the space integrals in the inner products of Eqs. (3.20) can eliminate the t dependence, and one obtains a constant value for each of these forcing terms. These terms will generate secular and even quadratic growth in Φ's expansion coefficients c_{nk}, which will invalidate the perturbation series (3.1). To suppress this growth, we need to impose the condition

$$d_{nk} = 0, \quad n = 1,...6, \quad k = 1,2. \tag{3.22}$$

These conditions will completely determine the slow time evolution of the soliton parameters. Indeed, when Eqs. (3.22)

are inserted into Eqs. (3.20), such evolution equations will be obtained. When the original time variable is restored, and Eqs. (3.2) used, these evolution equations can be written as

$$r_{kt} = \frac{\epsilon}{4}(R, \Psi_{\zeta_k}), \tag{3.23a}$$

$$v_{kt} = \frac{\epsilon}{4}(R, \Psi_{\xi_k}), \tag{3.23b}$$

$$\xi_{kt} = -2 r_k v_k - \frac{\epsilon}{4}(R, \Psi_{v_k}), \tag{3.23c}$$

$$\zeta_{kt} = r_k^2 - v_k^2 - \cos 2\theta_k \delta_{kt} - \frac{\epsilon}{4}(R, \Psi_{r_k}), \tag{3.23d}$$

$$\theta_{kt} = \frac{4 \cos 2\theta_k r_{kt} - \epsilon(R, \Psi_{\delta_k})}{8 r_k \sin 2\theta_k}, \tag{3.23e}$$

$$\delta_{kt} = \frac{\epsilon(R, \Psi_{\theta_k})}{8 r_k \sin 2\theta_k}. \tag{3.23f}$$

Integration of these differential equations will determine the evolution of the soliton parameters throughout collision.

With some more effort, the evolution of the continuous modes in the solution (3.18) can be similarly obtained. But this lies outside the scope of the present paper.
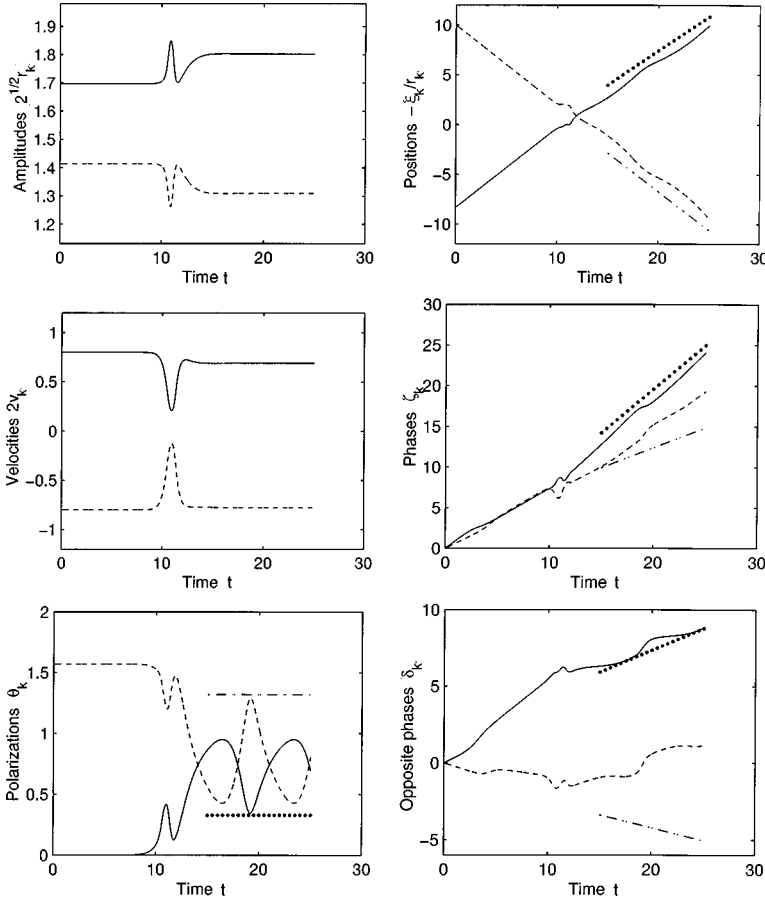
FIG. 2. Time evolution of the soliton parameters throughout collision for $\beta = 2/3$ and $v = 1.6$, predicted analytically by Eqs. (4.3). The solid and dashed curves are parameters of the first and second vector solitons, respectively. The dotted and dash-dotted curves are their shifted values after transmission (see the text for details).

IV. SOLITON COLLISIONS IN THE CNLS EQUATIONS

In polarization-maintaining birefringent fibers, pulses along the two orthogonal polarization axes are governed by the following CNLS equations:

$$iA_t + A_{xx} + (|A|^2 + \beta|B|^2)A = 0, \qquad (4.1a)$$

$$iB_t + B_{xx} + (|B|^2 + \beta|A|^2)B = 0. \qquad (4.1b)$$

Here we did not explicitly include the group velocity terms. The reason is that such terms can be eliminated by a simple phase transformation (see, e.g., Ref. [34]), not that we wanted to neglect them. But we did neglect the attenuation, higher-order dispersion and Raman effect. For soliton switching devices, this approximation is justified, since these effects are weak, and the switching fibers are short. However, for long-distance communication systems, the approximation needs careful scrutiny. For linearly birefringent fibers, the XPM coefficient β is 2/3. This is the case in logic gates and switches. For elliptically birefringent fibers, β will take other values [6]. In telecommunication fibers, the birefringence is random. In that case, β is averaged to be one. Meanwhile, the linear and nonlinear polarization mode dispersion terms will appear on the right-hand side of Eqs. (4.1) [8,9]. In this section, we only consider the polarization-maintaining fibers, where Eqs. (4.1) are the appropriate model.

Comparing Eqs. (4.1) to Eqs. (1.1), we see that

$$\epsilon = 1 - \beta, \quad M = |B|^2 A, \quad N = |A|^2 B. \qquad (4.2)$$

Thus the evolution equations (3.23) for the soliton parameters reduce to

$$r_{kt} = \frac{1 - \beta}{4} I_{\zeta_k}, \qquad (4.3a)$$

$$v_{kt} = \frac{1 - \beta}{4} I_{\xi_k}, \qquad (4.3b)$$

$$\xi_{kt} = -2 r_k v_k - \frac{1 - \beta}{4} I_{v_k}, \qquad (4.3c)$$

$$\zeta_{kt} = r_k^2 - v_k^2 - \cos 2\theta_k \delta_{kt} - \frac{1 - \beta}{4} I_{r_k}, \qquad (4.3d)$$

$$\theta_{kt} = \frac{4 \cos 2\theta_k r_{kt} - (1 - \beta) I_{\delta_k}}{8 r_k \sin 2\theta_k}, \qquad (4.3e)$$

$$\delta_{kt} = \frac{(1 - \beta) I_{\theta_k}}{8 r_k \sin 2\theta_k}, \qquad (4.3f)$$

where

$$I = I(r_k, v_k, \xi_k, \zeta_k, \delta_k, \quad k = 1,2) = \int_{-\infty}^{\infty} |A_h B_h|^2 dx. \qquad (4.4)$$

For simplicity, we consider the collision of two initially orthogonal vector solitons, with $\theta_1 = 0$ and $\theta_2 = \pi/2$. In this
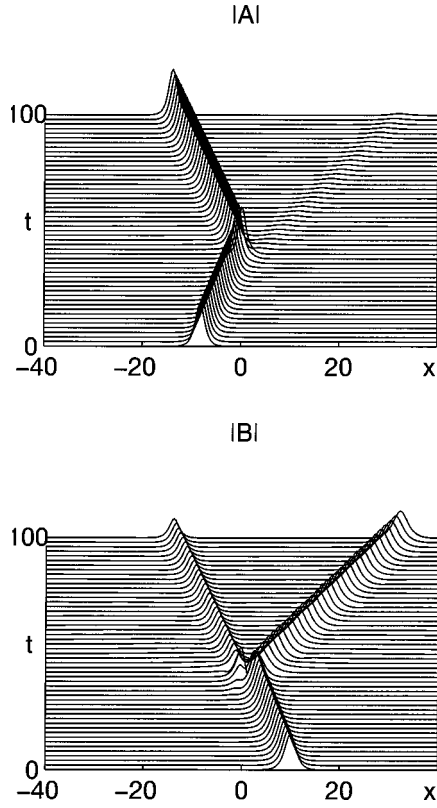
2400 JIANKE YANG PRE <u>59</u>

FIG. 3. Numerical simulation of Eqs. (4.1) with $\beta=2/3$ and $v=0.4$. The initial condition is given by Eqs. (4.5) with other parameters specified in the text.

FIG. 4. Numerical simulation of Eqs. (4.1) with $\beta=2/3$ and $v=1.6$. The initial condition is given by Eqs. (4.5).

case, the initial phase constants ζ_{k0} and δ_{k0} ($k=1$ and 2) can be scaled out. Thus, before collision, the two solitons (2.14) can be rewritten as

$$A(x,t)=\sqrt{2}r_1 e^{i\{v_1 x+(r_1^2-v_1^2)t\}}\, \mathrm{sech}(r_1 x-2r_1 v_1 t+\xi_{10}),$$
$$(4.5a)$$

$$B(x,t)=\sqrt{2}r_2 e^{i\{v_2 x+(r_2^2-v_2^2)t\}}\, \mathrm{sech}(r_2 x-2r_2 v_2 t+\xi_{20}).$$
$$(4.5b)$$

Without loss of generality, we take $v_1=-v_2=v/4(>0)$. So the approaching velocity of the two solitons is v. We also fix $r_1=1.2$ and $r_2=1$, so the initial amplitudes of the two solitons are approximately 1.6971 and 1.4142, respectively. They are chosen different so that we can track and identify them after collision. The choices for the initial position parameters ξ_{10} and ξ_{20} can be totally arbitrary. They will not
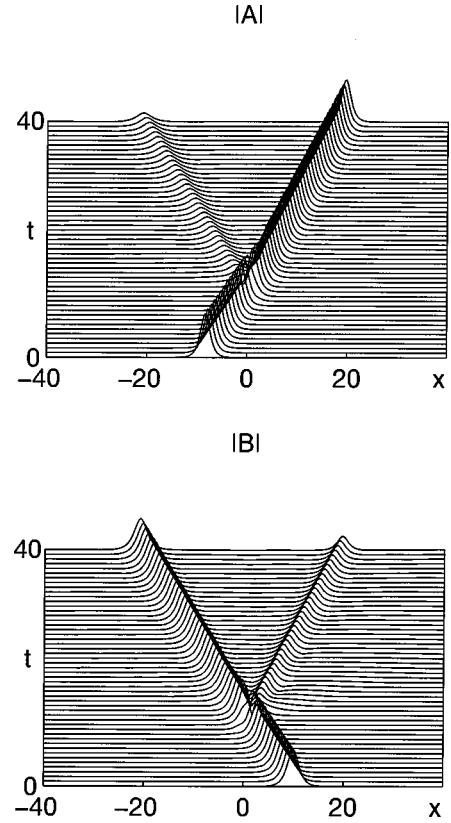
affect the collision outcome as long as $\xi_{10}>0$ and $\xi_{20}<0$ are large enough. We fix $\xi_{10}=10$ and $\xi_{20}=-10$ in our calculations. Thus, the two solitons are initially located at $x=-\xi_{10}/r_1\approx-8.33$ and $-\xi_{20}/r_2=10$, respectively. The only free parameters left are the XPM coefficient β and the collision velocity v, which will be used as control parameters. For given β and v values, we numerically integrate Eqs. (4.3) by the adaptive Runge-Kutta-Fehlberg method. Note that $\theta_k=0$ and $\pi/2$ are singular values in these equations. In order to initiate the integration, we actually took $\theta_1=10^{-6}$ and $\theta_2=\pi/2-10^{-6}$. Other choices of θ_1 and θ_2 values very close to 0 and $\pi/2$, respectively, do not affect the results. The integral I in Eq. (4.4) is evaluated by the trapezoidal rule with error control. The overall accuracy of our computations is about 10^{-5}.

We first carry out two individual computations to show typical evolutions of soliton parameters throughout collision. In the first case, we select $\beta=2/3$, which corresponds to linearly birefringent fibers, and $v=0.4$, which gives the ap-

TABLE I. Comparison between numerical and analytical values of the soliton parameters after collision. The initial conditions are given by Eqs. (4.5) with other parameters specified in the text.

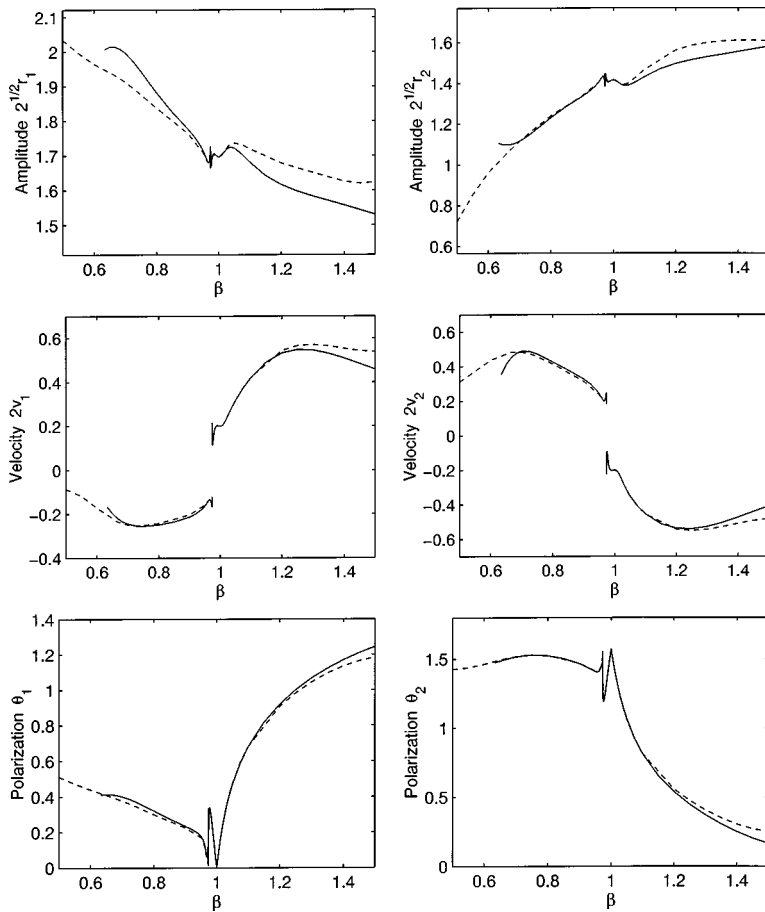|		r_1	v_1	θ_1	r_2	v_2	θ_2
case 1:	analytical	1.4240	−0.1096	0.4120	0.7760	0.2268	1.4963
$\beta=2/3$, $v=0.4$	numerical	1.3652	−0.1148	0.3982	0.7557	0.2448	1.5026
case 2:	analytical	1.2746	0.3448	0.3276	0.9254	−0.3885	1.3192
$\beta=2/3$, $v=1.6$	numerical	1.223	0.316	0.325	0.891	−0.363	1.297

FIG. 5. Amplitudes, velocities, and polarizations of the two postcollision vector solitons against β (the collision velocity v is fixed to be 0.4). The solid lines are from analytical predictions, and the dashed ones are from numerical simulations.

proaching velocity 0.4. For these values, the evolution of the soliton parameters are shown in Fig. 1. We observe that collision takes place at $t \approx 40$. During collision, the velocity of the right-moving soliton steadily decreases, and becomes negative when it emerges from the collision. This means that this soliton is reflected back by collision (this can be seen from the position plots as well). The same happens to the other soliton. It initially moves to the left, but turns around after collision. This reflection scenario has been reported in [23,25]. It is entirely due to the perturbations (4.2), because without them, the two solitons would pass through each other (see Sec. II). The amplitudes of the two solitons also changed after collision: the larger soliton gets even larger, and the smaller one gets even smaller. Thus energy has been transferred from the smaller soliton to the larger one. Additionally, the polarizations of the two solitons also shifted. This means that the energy inside a vector soliton has been partially transferred from one polarization axis to the other due to the collision. This is the so-called daughter wave (or shadow) creation discussed in [25].

If we increase the colliding velocity v, we expect the two solitons to pass through each other. This is indeed the case. For $\beta = 2/3$ and $v = 1.6$, the solutions of Eqs. (4.3) are shown in Fig. 2. We see that, when the solitons come into collision, their velocities decrease significantly as before. But in this case, they pick up speed again when they emerge from the collision. As a result, the solitons pass through each other, and settle down to constant speeds along the original directions. This transmission scenario has also been studied before [23–25]. The amplitudes of the two solitons underwent

similar changes as in the first case. One seemingly intriguing feature of this collision is that, after transmission, the polarization parameters θ_k do not approach constants, and the positions and phases ξ_k, ζ_k, and δ_k do not approach straight lines, as one would expect. Actually, this is easy to explain. Recall that these parameters correspond to those of the two separate solitons before collision [see Eqs. (2.14)]. After a transmissive collision, the values of ξ_k, ζ_k, θ_k, and δ_k are shifted (the amplitudes r_k and velocities v_k remain the same). These shifted values can be obtained from Eqs. (2.24) and (2.26). In Fig. 2, we also plotted these shifted parameters for the outcoming vector solitons. They behave as expected. Notice that the polarizations of the transmitted solitons have shifted away from 0 and $\pi/2$. This is the same daughter wave creation mentioned earlier. It is caused by the perturbations (4.2), because in the Manakov model, two initially orthogonal vector solitons do not change their polarizations after transmission (see Sec. II). If transmission does not take place, there are no such shifts in the soliton parameter values. This is why in the first case the parameter values shown in Fig. 1 are the actual ones of the reflected vector solitons.

To check the above analytical results, we directly simulated the CNLS (4.1) with the initial conditions as given by Eqs. (4.5). Our numerical scheme is the pseudospectral method in space, and the Runge-Kutta method in time. The results for both cases discussed above are plotted in Figs. 3 and 4, respectively. As predicted, the reflection scenario is observed in Fig. 3, while the transmission scenario is seen in Fig. 4. The quantitative comparison between numerical and analytical values of the soliton parameters after collision are
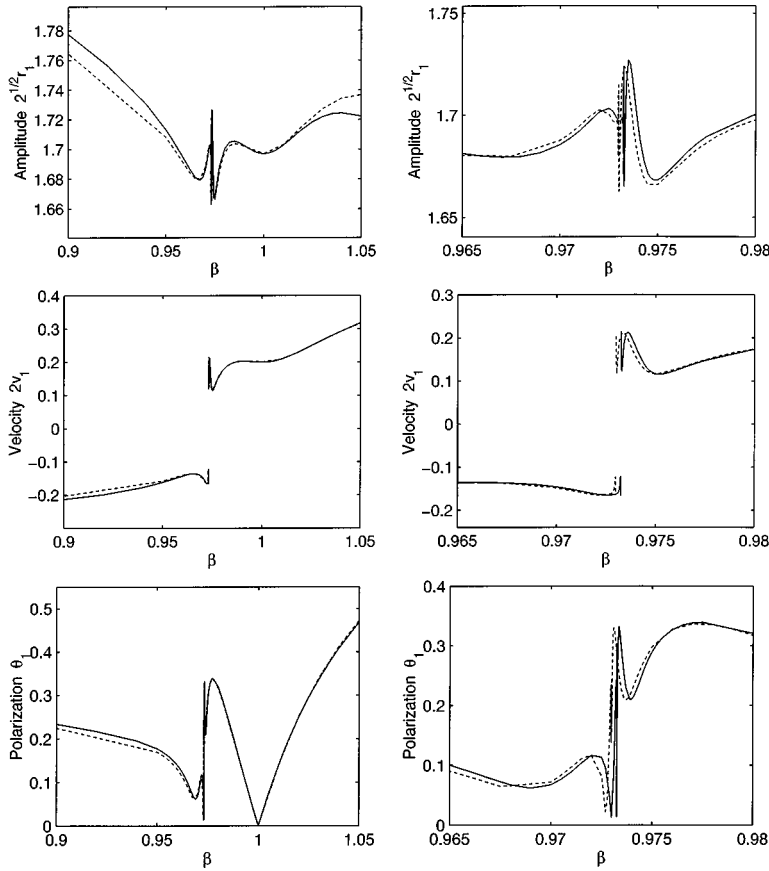
FIG. 6. Magnifications of the transition regions in the left half of Fig. 5. Notice that fast oscillations appear every time we zoom in.

shown in Table I. We see that the agreement is quite satisfactory, considering that the perturbations in these cases are not really small ($\epsilon = 1/3$).

Next, we systematically study the postcollision vector solitons as β or v continuously varies. We first fix the collision velocity $v = 0.4$, and integrate Eqs. (4.3) for various β values. The parameters of the vector solitons after collision against β are plotted in Fig. 5 (solid curves). The following features can be observed. (1) For smaller β values, the soliton velocities after collision have the opposite sign of their original ones. This simply means that the solitons are reflected by collision. For larger β values, the velocities after collision are of the same sign as their original ones. Thus the solitons pass through each other after collision. The transition from reflection to transmission takes place at $\beta_c \approx 0.9733$. (2) At smaller β values, the larger of the colliding solitons gets even larger, and the smaller of them gets even smaller, after collisions. In other words, in this case, collision transfers energy from the smaller soliton to the larger one. At larger β values, it is just the opposite. (3) After collision, the polarizations of the vector solitons are generally shifted away from 0 and $\pi/2$. In particular, for smaller β values, each of the two solitons after collision still retains most of its energy in the original polarization axis in which energy is launched (since the polarization shift is less than $\pi/4$). But for larger β values, the solitons can transfer most of their energy to the opposite polarization axes by collision. (4) When β decreases below roughly 0.75, the velocities of the reflected solitons start to get smaller. This suggests that for a certain range of small β values, the velocities of the reflected solitons may become zero, thus the two solitons will fuse into one after collision. This is indeed the case (see the end

of this section and also Fig. 8). When β further decreases close to zero, the collision will be transmissive again. The reason is that, when $\beta = 0$, the CNLS (4.1) become two decoupled NLS, and the two orthogonal solitons (4.5) will pass by each other with no collision at all. But these β regimes lie outside the scope of the present perturbation theory. (5) In the θ_1 and θ_2 plots, there are sharp corners near $\theta_1 = 0$ and $\theta_2 = \pi/2$. This is because we restricted the soliton polarizations to be in the interval $[0, \pi/2]$. Without this restriction, such spikes would disappear.

Another noticeable feature in Fig. 5 is that the transition from reflection to transmission is not a smooth process. In fact, as β approaches β_c from either side, the soliton parameters after collision start to oscillate, and the oscillating frequency gets higher and higher. To see it more clearly, we twice magnify the transition regions in the first soliton's parameters and plot them in Fig. 6. Each time we zoom in, we see new and faster oscillations emerging. This process appears to continue indefinitely. The oscillation amplitudes in r_1, v_1, and θ_1 are about 4%, 50%, and 200% of their average values, respectively. Thus, in the transition region, the outcoming solitons are very sensitive to the β value. Slight changes in β could alter the outcoming soliton parameters significantly. Similar behaviors are observed for the second soliton as well. It makes the prediction of the vector solitons after collision somewhat uncertain in the transition region. This uncertainty is especially serious in the velocities and polarizations of the outcoming vector solitons because of the relatively large and rapid oscillations in those parameters.

All these analytical predictions have been verified by direct numerical simulations. In Figs. 5 and 6, the numerically obtained soliton parameters after collision are also plotted
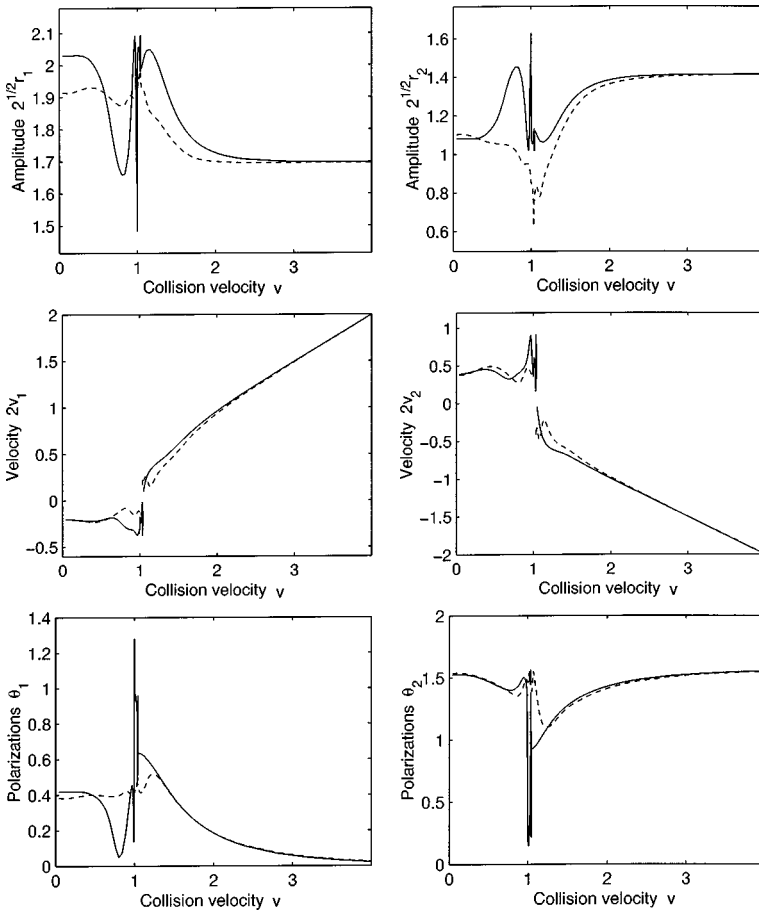
FIG. 7. Amplitudes, velocities, and polarizations of the postcollision vector solitons against the initial collision velocity v (β is now fixed to be 2/3). The solid lines are from analytical predictions, and the dashed ones from numerical simulations.

for comparison. We see that when β is close to 1, which is the regime where the above perturbation theory is based, the agreement between the numerical and analytical values is very good (as expected). This agreement deteriorates when β moves away from 1, but is still satisfactory over a broad range of β values centered around 1. In particular, the numerical results confirmed the jittery transition from reflection to transmission, which was predicted analytically (see Fig. 6). The numerical β_c value for transition is $\beta_c \approx 0.9730$, which agrees remarkably well with the analytical β_c value.

Next, we fix $\beta = 2/3$, and study the vector solitons after collision for various collision velocities v. The analytical soliton parameters are obtained by integrating Eqs. (4.3) and applying the shift formulae in Sec. II in the case of a transmissive collision. These results are shown in Fig. 7 (solid curves). Also plotted are the numerical values (dashed curves) for comparison. At small collision velocities, the collision is reflective, while at large collision velocities, it is transmissive. The transition value v_c is predicted to be 1.05, which can be compared to the numerical value 1.03. One interesting feature in Fig. 7 is that, when $v \rightarrow 0$, the parameters of the reflected solitons approach certain limits. For instance, we analytically predict that the velocities $2v_1$ and $2v_2$ approach -0.2046 and 0.3892, respectively. It is verified by the numerical results (see Fig. 7). This means that, for a slow collision, no matter how slow it is, the collision outcome is always the same. In particular, the outcoming vector solitons always move at fixed nonzero speeds. This is quite remarkable. Another feature in Fig. 7 is that, as v gets larger, the soliton parameter values after collision get closer

to their original ones. This is expected, since when v is larger, the collision is faster, and thus weaker. As a result, the solitons will change less in such a collision. One more feature in Fig. 7 is that the transition from reflection to transmission is also sensitive and oscillating rapidly, just as in the first case. In this region, the analytical and numerical values do not match well: the numerical curves are less violent. The reason is twofold. First, the perturbation parameter $\epsilon = 1/3$ is not very small here. Thus the theoretical results are subject to errors of that order. Second, the soliton parameters in this region are sensitive to the v value. Nonetheless, the analytical curves still qualitatively capture the overall features of the numerical ones.

From the above results, we conclude that the present perturbation theory successfully describes the reflection and transmission scenarios of the collision for β close to 1. But there are other collision scenarios, notably fusion and creation of new vector solitons, which may occur at β values far away from 1. The present theory is inadequate in describing them. Fusion typically occurs when β is small, and the collision is slow. One example, with $\beta = 0.3$ and $v = 0.4$, is shown in Fig. 8. Creation of new vector solitons can happen when β is large, and the collision velocity is moderate. An example, with $\beta = 3$ and $v = 1.6$, is shown in Fig. 9. We will discuss such collisions elsewhere.

Finally, we wish to compare the above collision results in the CNLS equations to those between kink and antikinks in the ϕ^4 nonlinear Klein-Gordon equations. In the ϕ^4 theory, two types of collision scenarios between a kink and an antikink have been reported [35,36]. One is reflection, in which
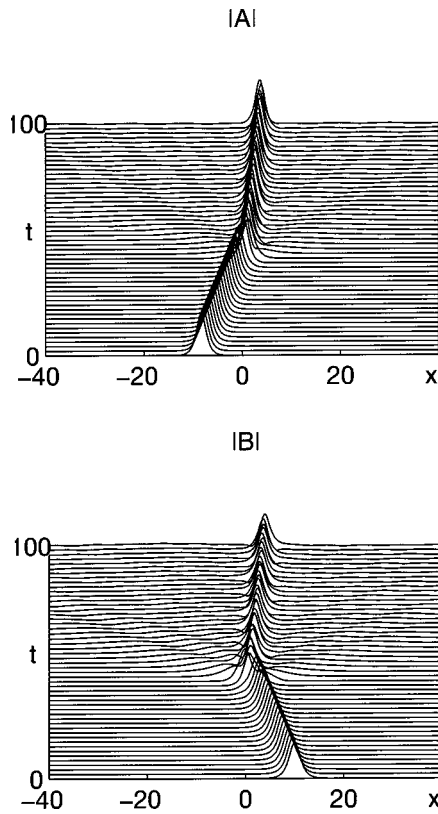
|A|

|B|

FIG. 8. Fusion of two solitons into one in the CNLS (4.1) (numerical simulations). The initial conditions are given by Eqs. (4.5) with $\beta = 0.3$ and $v = 0.4$.
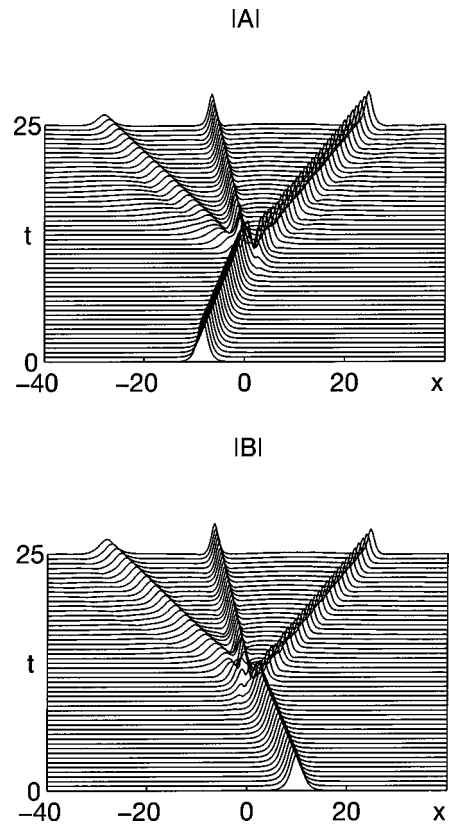
|A|

|B|

FIG. 9. Creation of new vector solitons after collision in the CNLS (4.1) (numerical simulations). The initial conditions are given by Eqs. (4.5) with $\beta = 3$ and $v = 1.6$.

the kink and antikink are reflected from each other. This happens for large collision velocities. The other is fusion, in which the kink and antikink capture each other and form a long-lived, spatially localized, time-oscillatory state. This occurs for small collision velocities. In the transition region, intervals of collision velocity for fusion and reflection alternate with each other. This alternation gets faster and faster as the collision velocity approaches a critical value. This so-called resonance structure was explained semianalytically in [35]. The basic idea is that there exists an internal mode for the kink and antikink in the ϕ^4 equation. During collision, this mode can temporarily store energy taken away from the colliding waves' kinetic energy, and give it back when the collision is over. In our results for the CNLS equations, we also identified two collision scenarios: transmission and reflection. In the transition region, we observed oscillations in the parameters of the outcoming solitons. This is reminiscent of the behavior in the ϕ^4 theory. Furthermore, we have discovered recently that internal modes also exist for vector solitons in the CNLS equations [37]. This raises a strong possibility that the resonance mechanism proposed in [35] may also be at work here. But for the parameter values we chose, the transition is clear-cut. There is no alternation between parameter intervals for transmission and reflection. It would be interesting to see if this will change when the initial soliton parameters are varied. To answer this question, substantially more numerical and analytical work will be needed.

V. DISCUSSION

In the previous sections, we analytically studied the collision of vector solitons in the perturbed Manakov equations, and applied the results to the collision of orthogonally polarized solitons in the CNLS equations. We showed that, in the presence of perturbations, the soliton parameters, such as the amplitudes, velocities, and polarizations, will change after collision. We found that both transmissive and repulsive collisions can occur, depending on the combinations of initial parameter values. In the region of transition from transmission to reflection, the collision outcome is sensitive to the parameters of colliding solitons and the XPM coefficient β. Considerable oscillations were observed in the parameters of the outcoming vector solitons. These results were compared to the direct numerical simulations, and very good agreement was demonstrated.

Next we discussed the applications of these results to optical switches. We have shown above that, for relatively small collision velocities, the orthogonally polarized solitons in polarization-maintaining fibers undergo reflective collision (see Figs. 3 and 7). This suggests the interesting possibility of designing the soliton-repulsion logic gate using birefringent fibers (such a logic gate using dual-core fibers or beams in crystals has been proposed recently in [38,12]). In this logic gate, the control and signal pulses are launched successively along the fast and slow polarization axes of the birefringent fiber. If the relative group velocity of the two pulses is moderately small, then they will be reflected by each other after collision. This reflective collision significantly increases

the position and frequency (velocity) shifts of the pulses. As a result, shorter polarization-maintaining fibers may be needed to create the required amount of position or polarization shift for switching. In addition, this logic gate is phase independent and cascadable. We will investigate this type of logic gate further elsewhere.

[1] A. Hasegawa and F. Tappert, Appl. Phys. Lett. **23**, 142 (1973).

[2] L. F. Mollenauer, R. H. Stolen, and J. P. Gordon, Phys. Rev. Lett. **45**, 1045 (1980).

[3] V. E. Zakharov and A. B. Shabat, Zh. Eksp. Teor. Fiz. **61**, 118 (1971). [Sov. Phys. JETP **34**, 62 (1972)].

[4] M. J. Ablowitz and H. Segur, *Solitons and the Inverse Scattering Transform* (SIAM, Philadelphia, 1981).

[5] C. R. Menyuk, IEEE J. Quantum Electron. **QE-23**, 174 (1987).

[6] C. R. Menyuk, IEEE J. Quantum Electron. **QE-25**, 2674 (1989).

[7] C. R. Menyuk, J. Opt. Soc. Am. B **5**, 392 (1988).

[8] P. K. A. Wai and C. R. Menyuk, J. Lightwave Technol. **LT-14**, 148 (1996).

[9] T. I. Lakoba and D. J. Kaup, Phys. Rev. E **56**, 6147 (1997).

[10] J. U. Kang, G. I. Stegeman, J. S. Aitchison, and N. Akhmediev, Phys. Rev. Lett. **76**, 3699 (1996).

[11] A. Villeneuve, J. U. Kang, J. S. Aitchison, and G. I. Stegeman, Appl. Phys. Lett. **67**, 760 (1995).

[12] S. Blair, K. Wagner, and R. McLeod, J. Opt. Soc. Am. B **13**, 2141 (1996).

[13] D. J. Benney and A. C. Newell, J. Math. Phys. **46**, 133 (1967).

[14] G. J. Roskes, Stud. Appl. Math. **55**, 231 (1976).

[15] M. N. Islam, *Ultrafast Fiber Switching Devices and Systems.* (Cambridge University Press, New York, 1992).

[16] K. H. Ahn, M. Vaziri, B. C. Barnett, G. R. Williams, X. D. Cao, M. N. Islam, B. Malo, K. O. Hill, and D. Q. Chowdhury, J. Lightwave Technol. **LT-14**, 1768 (1996).

[17] S. G. Evangelides, L. F. Mollenauer, J. P. Gordon, and N. S. Bergano, J. Lightwave Technol. **LT-10**, 28 (1992).

[18] L. F. Mollenauer, J. P. Gordon, and F. Heismann, Opt. Lett. **20**, 2060 (1995).

[19] J. P. Silmon-Clyde and J. N. Elgin, Opt. Lett. **23**, 180 (1998).

[20] S. Blair, K. Wagner, and R. McLeod, Opt. Lett. **19**, 1945 (1994).

[21] S. V. Manakov, Zh. Eksp. Teor. Fiz. **65**, 505 (1973) [Sov. Phys. JETP **38**, 248 (1974)].

[22] R. Radhakrishnan, M. Lakshmanan, and J. Hietarinta, Phys. Rev. E **56**, 2213 (1997).

[23] B. A. Malomed and S. Wabnitz, Opt. Lett. **16**, 1388 (1991).

[24] C. Sophocleous and D. F. Parker, Opt. Commun. **112**, 214 (1994).

[25] J. Yang and D. J. Benney, Stud. Appl. Math. **96**, 111 (1996).

[26] Y. S. Kivshar and B. A. Malomed, Rev. Mod. Phys. **61**, 763 (1989).

[27] D. J. Kaup, Phys. Rev. A **42**, 5689 (1990).

[28] Y. Matsuno, Phys. Rev. E **51**, 1471 (1995).

[29] Y. Matsuno and D. J. Kaup, J. Math. Phys. **38**, 5198 (1997).

[30] J. Yang and D. J. Kaup (unpublished).

[31] M. Midrio, S. Wabnitz, and P. Franco, Phys. Rev. E **54**, 5743 (1996).

[32] V. S. Shchesnovich and E. V. Doktorov, Phys. Rev. E **55**, 7626 (1997).

[33] J. P. Keener and D. W. McLaughlin, Phys. Rev. A **16**, 777 (1977).

[34] D. J. Kaup and B. A. Malomed, Phys. Rev. A **48**, 599 (1993).

[35] D. K. Campbell, J. F. Schonfeld, and C. A. Wingate, Physica D **9**, 1 (1983).

[36] M. J. Ablowitz, M. D. Kruskal, and J. R. Ladik, SIAM (Soc. Ind. Appl. Math.) J. Appl. Math. **36**, 428 (1979).

[37] J. Yang, Stud. Appl. Math. **98**, 61 (1997).

[38] Y. Oh, J. W. Haus, and R. L. Fork, Opt. Lett. **21**, 315 (1996).